doi:10.14311/ppt.2025.3.208
Plasma Physics and Technology **12**(3):208–213, 2025

INFLUENCE OF RADIATION ENERGY LOSSES IN A NUMERICAL SIMULATION OF SUBSONIC VACUUM ARC IN THE PRESENCE OF AN EXTERNAL AXIAL MAGNETIC FIELD.

C. Simonnet[a,*], P. Freton[a], J.J. Gonzalez[a], F. Reichert[b], A. Petchanka[b]

[a] *Laboratoire plasma et conversion d'énergie (Laplace) UMR 5213 - CNRS - Toulouse INP - UT3 Université Toulouse 3 - Paul Sabatier 118, route de Narbonne - bât 3R3 - 31062 Toulouse cedex 9, France*

[b] *Siemens Energy, Paulsternstr. 26, 13629, Berlin, Germany*

[*] `claire.simonnet@laplace.univ-tlse.fr`

Abstract.

We present a three-dimensional (3D) Magneto Hydrodynamic Model (MHD) at two temperatures (electronic and ionic) of inter-electrodes plasma, simulated with Ansys Fluent coupled with specific developments in C language. The stationary model describes a subsonic arc in vacuum at 15 kA between copper contacts, submitted to an Axial Magnetic Field (AMF). Due to high temperatures, losses by radiation need to be considered. Even if departures from Local Thermal Equilibrium (LTE) exist, currently due to lack of appropriate data, net emission coefficient data calculated under LTE are used and attributed exclusively to electron energy equation. Two cases are investigated in this study, with or without considering the radiation in the electrons energy equation. The study highlights the importance of better characterizing radiative losses in order to improve the reliability of numerical models.

Keywords: electric arc, vacuum, simulation, AMF, radiation.

1. Introduction

The study of high voltage circuit breakers using vacuum as a breaking medium has gained renewed interest in recent years [1]. With increasing demands to reduce greenhouse gas emission, these technologies are the focus of new research, particularly for high voltage and high current applications (beyond 1 kV, several tens of kA). In a vacuum circuit breaker, we find the vacuum tube in which the arc is created by the contact separation during the switching-off process [2]. Understanding the behavior of the vacuum arc remains a challenge, especially under initial pressure (about 10^{-5} Pa) and high current conditions. In these conditions, experimental measurements are limited and do not allow access to arc behavior [3]. When the contacts open an electric arc is established containing vapors from the erosion of the electrodes (mainly cathode). This arc can operate in diffuse supersonic mode (at low intensity) or concentrated mode (at high intensity) [4]. To avoid plasma contraction and contact overheating, an axial magnetic field (AMF) can be applied [5]. Specific contact designs allow a distribution of the current path more homogeneously. Three other arc modes exist by applying an AMF: multiple arc, subsonic diffuse arc and diffuse columnar [4]. This study focuses on the subsonic mode of the electric arc. In the literature, the main presented models [6–8] do not take radiation losses into account. When these losses are taken into account, as for example in E. Schade [4], the author do not specify how these data are used. In this context, we present a 3D model based on a MHD approach of an inter-electrode plasma at two temperatures (electronic and ionic). We will explain how radiation energy losses have been taken into account in our model and how they affect stationary simulation results in literature conditions [4].

2. Two-temperature electric arc model in vacuum

We present the chosen approach inspired by the literature to represent the vacuum electric arc completed by energy losses by radiation. We use Ansys Fluent with developments (in C language) containing UDFs (User Defined Functions) and UDSs (User Defined Scalars) to describe the physics of the electric arc [9].

2.1. Configuration

Due to the use of an AMF, the electrodes have complex geometries [2, 10]. However in numerical models, simplified geometries are considered [4, 6, 7], namely flat electrodes to facilitate calculations in a first approach. The geometry of arc domain classically studied in the literature is a cylinder, and the model based on the equations presented by Braginskii [11]. In our study, we consider two flat parallel copper electrodes, with a diameter equal to 50 mm and separated by 10 mm (Figure 1). The anode (top), the cathode (bottom) are not modeled but are taken into account via specific

boundary conditions (BC). An AMF denoted $\vec{B}_{AMF}$ is applied in the inter-electrode space .

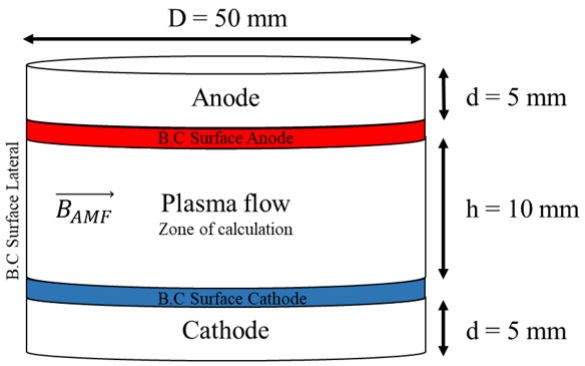

Figure 1. Geometry studied.

2.2. Hypotheses

We consider a 3D laminar [4] model in stationary state. The plasma is a fully ionized mixture of electrons and copper ions (Cu^+, Cu^{2+}, Cu^{3+}) of respective masses m_e and m_i, with an average charge fixed at $Z = 1.9$ [12, 13]. It is assumed quasi-neutral, with an electron density $n_e = Zn_i$. Neutral particles are not considered. The mean free path of charged particles λ (ions-ions $\lambda_{ii} = 10^{-5}$ m, electrons-electrons $\lambda_{ee} = 10^{-7}$ m) remains small compared to the characteristic dimensions [14]. Under these conditions, considering $L = 1$ cm the characteristic length of the system, the Knudsen number $K = \frac{\lambda}{L} \ll 1$ for electrons and ions, corresponding to a continuous medium, which justifies the use of the fluid model. The latter are assumed to behave like ideal gases. The plasma is not in thermal equilibrium: ions and electrons each have their own temperature (T_i, T_e) and follow a Maxwellian distribution. An uniform AMF is imposed, with a value typically used in the literature of 5 mT/kA [4]. For example, for a current of 15 kA, the field reaches 75 mT. Anisotropic electronic conductivity, due to the presence of an AMF, is also taken into account [4].

2.3. Boundary conditions

The cathode is considered to be a mass flux inlet, with a BC of Gaussian profile of current density. This profile is adjusted so that the intensity at the cathode edge represents approximately 10 % of that at the center. Plasma heavy particles originate from cathode erosion, with an imposed mass flux [6]. According to C. W. Kimblin [15], the copper erosion rate varies between 35 and 40 µg/C, but a value of 50 µg/C is used here, based on more recent studies [16]. In accordance with the work of E. Schade [4] and almost all papers of the literature, we assume the electron and ion temperatures equal to 3 eV.

The anode collects the plasma flux and is considered as an outlet with a flux condition. The anode outlet pressure, corresponding to the total pressure, is calculated from the ion velocity, using a method derived from the work of Y. Langlois's [6]. The anode potential is also calculated using a method inspired by Tezenas [7], using the total current and sheath components. At the edges of the plasma domain, we consider a zero flux. The emission of metal vapors is not taken into account; the anode is passive. An anode sheath regulates the electron and ion fluxes, and a specific potential is associated with it [6].

3. Equations and energy losses due to radiation

The magneto hydrodynamic equations are linked with Maxwell's equations. The system of equations established for two fluids at two temperatures is presented in a previous paper [17]. We are particularly interested by the term of energy losses by radiation. The resolution of the energy equation of electrons, like ions, is treated as a function of the mass enthalpy. The mass enthalpy of electrons is given by the following relation with m_i the ions mass and k_B the Boltzamnn constant:

$$h_e = \frac{5}{2} \cdot \frac{k_B Z T_e}{m_i} \tag{1}$$

The electron energy equation is:

$$\begin{aligned} \nabla \cdot (\rho_i \vec{v}_e h_e) = \vec{v}_e \cdot \nabla P_e + \nabla \cdot (k_e \nabla T_e) \\ + \frac{j_x^2 + j_y^2}{\sigma_\perp} + \frac{j_z^2}{\sigma_\parallel} - Q_i + F_r - R \end{aligned} \tag{2}$$

We calculate the convective flow of electronic energy, i.e. convective enthalpy transport by electrons through this term $\nabla \cdot (\rho_i \vec{v}_e h_e)$, with ρ_i the mass density of ions, $\vec{v}_e$ vector velocity of electrons. To solve this equation we evaluate the source terms. Respectively on the right hand side of the equation 2 we have the convective term $\vec{v}_e \cdot \nabla P_e$, which represents the work forces applied to the electrons, with ∇P_e the pressure gradient of the electrons, the diffusive term $\nabla \cdot (k_e \nabla T_e)$, with k_e the thermal conductivity, the Joule terms $\frac{j_x^2+j_y^2}{\sigma_\perp} + \frac{j_z^2}{\sigma_\parallel}$, it corresponds to the ohmic heating term due to anisotropic electronic conductivity ($\sigma_\perp$ and $\sigma_\parallel$) which depends on the direction of the AMF [11] and $j_{x,y,z}$ are the components of the current density. Q_i is the exchange term of energy between electrons and ions.

The two last terms F_r [4, 11] and R correspond respectively to the friction term and to the losses of energy by radiation. In the literature, the energy losses by radiation, in a two-temperature arc plasma are not always considered. In its model, E. Schade [4] uses a net emission coefficient with a constant value of 10^{10} W/m^3 assigned to the electrons. In vacuum medium, the consideration of energy losses remains

relatively questionable as data calculation is based under LTE assumptions. The hypotheses established for the Net Emission Coefficient ϵ_n (NEC) calculation are described in Lowke work [18].

We present in Figure 2 the ionic and electronic temperature profiles in black and the absolute pressure in red. These profiles are taken at the center of the inter-electrode space at 0.5 cm from the electrodes. The current is 15 kA, the AMF= 75 mT, the ablation rate is 50 µg/C and the mean charge $Z = 1.9$, it's a reference case.

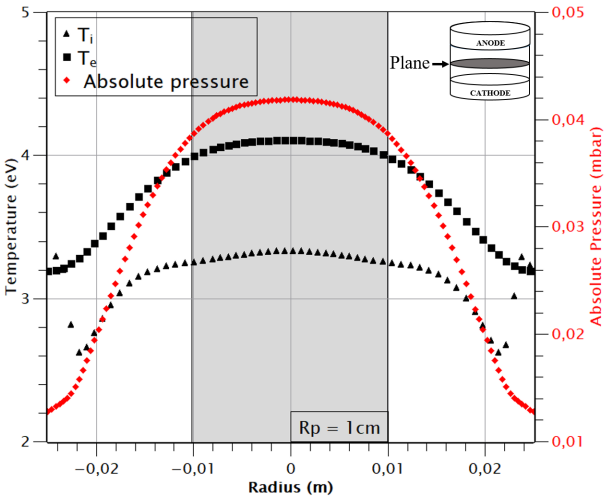

Figure 2. Profiles of ionic (black diamond) and electronic (black square) temperature in eV and absolute pressure (red diamond) as a function of radius at the center of the domain.

According to the two black curves (ion temperature diamond and electron temperature square), we consider that there is a weak temperature gradient at the center of the plasma over a radius of about 1 cm. This value $R_\mathrm{p} = 1$ cm is chosen to calculate the net emission coefficients. The relation between the divergence of the radiative flux $\nabla \cdot \vec{q}_\mathrm{r}$ and the NEC ϵ_n is as follows:

$$\nabla \cdot \vec{q}_\mathrm{r} = 4\pi\varepsilon_\mathrm{n} \tag{3}$$

To estimate $\epsilon_\mathrm{n}(T, R_p)$ we use this equation:

$$\varepsilon_\mathrm{n}(T, R_\mathrm{p}) = \int_0^\infty L_\nu^0(T) K_\nu'(T) \exp\left(-K_\nu'(T) R_\mathrm{p}\right) \mathrm{d}\nu \tag{4}$$

with $K_\nu'(T)$ the mean absorption coefficient [19], $\exp(-K_\nu'(T)R_\mathrm{p})\,\mathrm{d}\nu$ the absorption term, $L_\nu^0(T)$ the blackbody luminance (Planck function), R_p the radius of the NEC calculation sphere and $\mathrm{d}\nu$ the spectral interval. We use the Kurucz database [20] for the input data because they are more complete than the NIST [21] in Copper case at high temperatures even if some data are theoretical ones. We then estimate NEC by homemade soft. In Figure 3, we represent the variation of the net emission coefficient and its components for copper at a pressure of 0.01 bar for a radius of 1 cm depending on the electronic temperature.

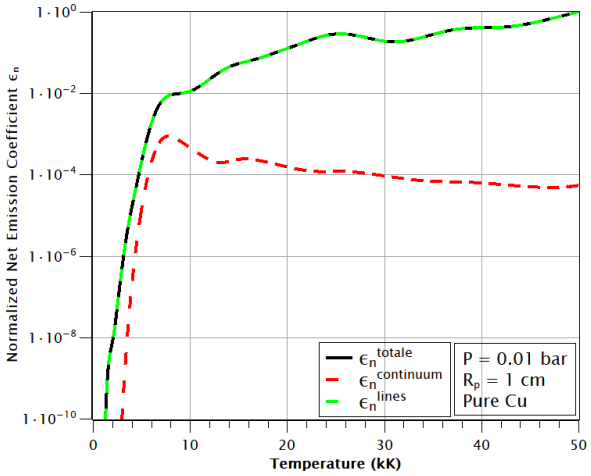

Figure 3. Net emission coefficient for copper at 0.01 bar for $R_p = 1$ cm depending on the temperature, normalized by the maximum value of the ϵ_n^{totale}. Continuum emission (in red) and lines (in green) by the dotted lines.

Electrons are lighter than ions, $m_\mathrm{e} \ll m_\mathrm{i}$, and the electron density is higher than the ion density, $n_\mathrm{e} = Zn_\mathrm{i}$. Electrons have a higher thermal velocity (which depends on their temperature), they incur the strongest accelerations, and they have a greater kinetic energy than ions. They cause the majority of radiant electronic transitions. They interact most efficiently with electromagnetic fields and are responsible for the excitation of ions. For the continuum, electrons are the main contributors to free radiation, bremsstrahlung, and recombination, and that of ions in a fully ionized plasma is negligible. For lines, the electrons control the excitation of the ion energy levels, which induces the emission of photons and therefore energy by radiation through de-excitation. We choose then to associate the radiation losses to the electrons and to consider the data (Figure 3) as a function of electronic temperature. For the pressure dependence, the following equation is used:

$$\varepsilon_\mathrm{n}(T, R_\mathrm{p}) = \frac{\varepsilon_\mathrm{n}(0.01) \cdot P\ (\mathrm{mbar})}{0.01\ \mathrm{bar}} \tag{5}$$

4. Simulation results

We now consider two cases: one with no radiation in the energy equation (reference case, left side in the figures), the second with radiation in the electron energy equation (right side in the figures). The field of the quantity considered is cut along the axis of revolution of the domain. The input data are the same as those of the reference case of the previous section. In Figure 4, we observe the energy exchange term Q_i characterized by the following equation:

$$Q_i = 3\frac{m_e n_e}{m_i \tau_e} k_B (T_e - T_i) \tag{6}$$

where τ_e is the relaxation time between two electron-electron collisions [11] and k_B is the Boltzmann constant.

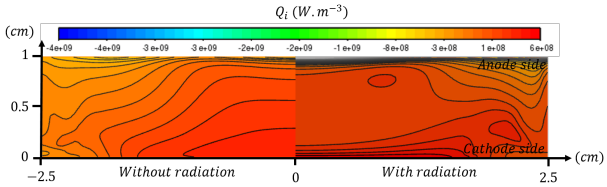

Figure 4. Fields of the Q_i exchange term in $W.m^{-3}$, on the left without radiation and on the right with radiation.

Considering radiative losses, the energy exchange term increases in the inter-electrode space except at the anode surface where this term decreases sharply. This can be seen in Figure 5 with the electronic temperature fields T_e in a) and ionic T_i in b). These radiative energy losses lead to a cooling of the plasma. In order to reduce the thermal imbalance, the electrons that are hotter than the ions will transfer more energy to the latter to compensate for the losses. At the anode surface, Q_i decreases sharply when T_i is greater than T_e, the presence of the positive anode sheath reduces the energy transfer to the slower ions [6].

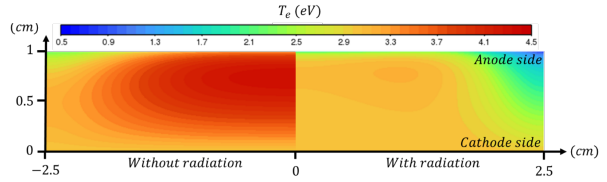

(a).

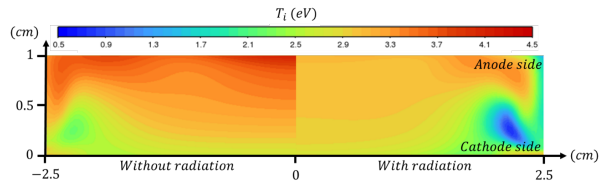

(b).

Figure 5. Electronic T_e a) and ionic T_i b) temperature fields in eV.

If the exchange term increases the difference between T_e and T_i is greater. We find a higher thermal imbalance than in case without radiative losses. Note that the ion velocity decreases at the edges of the domain, resulting in a decrease in T_i at this point in Figure 5b. We can also see in Figure 6, the profiles of the components of the anisotropic electrical conductivity at 5 mm from the electrodes at the center of domain, $\sigma_\perp$ and $\sigma_\parallel$ in S/m whose definitions come from the work of Braginskii [11].

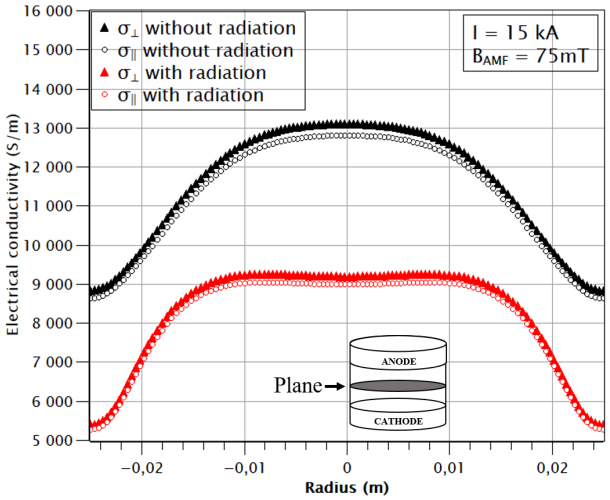

Figure 6. Profiles of anisotropic electrical conductivity with the quantities, $\sigma_\perp$ and $\sigma_\parallel$, in black without radiation and in red with radiation.

Conductivity is proportional to the temperature of the electrons, which decreases [6, 7]. The electrons have lost kinetic energy at the center of the plasma, so the conductivity decreases. The energy losses are higher; the potential difference increases and goes from 11 to 16 V.

As a result, the power increases leading to an augmentation of electron energy. At constant volume in the inter-electrode space, we expect an increase in the density of electrons n_e and ions n_i. The electron and ion densities increase with the inclusion of radiative losses due to the compression of the plasma in the center of the domain and the greater ionization phenomenon. Since the collision frequency is higher due to lower temperatures, the species densities increase, n_e is going from 6.10^{21} to 9.10^{21} m^{-3} in the center of the domain. Since the density increases in the center of the plasma, the pressure also follows this same trend as we can see in Figure 7. According to Dalton's law: $\sum_\alpha P_\alpha = \sum_\alpha k_B n_\alpha T_\alpha = k_B n_e T_e + k_B n_i T_i$, the pressure is a function of the density of the electronic and ionic temperatures of the plasma. We note that taking into account radiative losses, the pressure increases from about 40 mbar to 60 mbar in the tube.

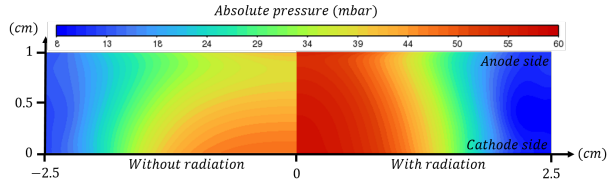

Figure 7. Absolute pressure field in mbar, left without radiation and right with radiation.

An increase in pressure in the domain and at the electrodes vicinity can induce a more concentrated and therefore more significant erosion at the anode. At the anode surface, the increase in pressure at the center of the domain leads to an increase in the energy

flux of the electrons and ions. The energy flux of a) electrons q_e and b) ions q_i in W/m^2 (given in Figure 8) were calculated from the following equations:

$$q_i = \Phi_i \left(\frac{5}{2} k_B T_i + \frac{m_i v_i^2}{2} + ZeU \right) \quad (7)$$

$$\Phi_i = n_i v_i \quad (8)$$

$$q_e = \Phi_e \left(2 k_B T_e + w \right) \quad (9)$$

$$\Phi_e = n_e \sqrt{\frac{k_B T_e}{2\pi m_e}} \exp\left(-\frac{eU}{k_B T_e} \right) \quad (10)$$

With v_i the speed of the ions, Z the average charge of the plasma, U the arc voltage at anode sheath (obtained from boundary condition as in B. Tezenas work [7]), Φ_e and Φ_i respectively the mass flow of electrons and ions, and $w = 4.5\,\text{eV}$ the electron work function [22]. In these expressions, the radiative contributions, to the anode and from the anode, are not taken into account. Indeed, using net emission coefficient method the radiation flux is not available on the anode surface. In case of thermal plasma at atmospheric pressure the electronic flux on the anode is on the same order of magnitude than the radiative contribution. So in the Figure 8a, in reality the energy flux of the electron considering radiation should be higher than the one given by the black curve. This radiative contribution should be added to the equation 9. At the moment, this is not the case, nevertheless in future work we plan to use other radiative methods as the discrete ordinate method (DOM) [23] to not only estimated the radiative terms but to take it into account during the direct calculation. This method necessitates the previous calculation of the mean absorption coefficients function of the temperature and pressure.

We can see in Figure 8a, that the electron energy flux is 25% lower when considering radiative losses showing the importance of the term in the transferred flux to the anode. Similarly, in Figure 8b, the ion energy flux is 10% lower when taking into account radiative losses. Indeed as the electron temperature is lower, the energy transferred by elastic collisions to the ions is weaker. The total power deposited by particles on the anode surface decreases with the consideration of radiative losses, it goes from 292 kW to 286 kW. The power deposited by the ions decreases by about 8 kW and that of the electrons increases slightly by 2 kW. An increase of total energy flux at the anode surface can reduce electrode life and the reliability of circuit breaker.

5. Conclusion

Two-temperature modeling of a subsonic vacuum arc, based on assumptions and theory from the literature, allowed us to obtain consistent results. However, we did not find any radiation data for a two-temperature plasma that allowed us to associate a contribution

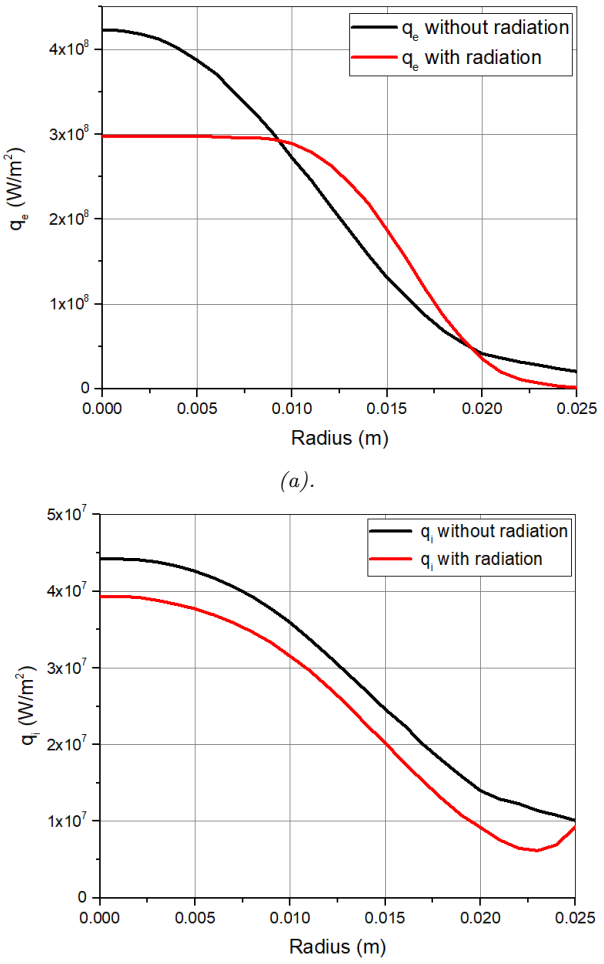

Figure 8. Energy flux of a) electrons and b) ions in $W.m^{-2}$, at anode surface.

for ions and another for electrons. The alternative chosen to estimate these losses is the net emission coefficient of copper, calculated at equilibrium and associated to the electrons. From this estimation, we showed the significant impact of taking into account radiation energy losses. In our case, this reduces the temperature of the species and favors an increase of pressure, arc voltage and energy flux of the particles to the anode.

References

[1] R. L. Boxman, S. Goldsmith, and A. Greenwood. Twenty-five years of progress in vacuum arc research and utilization. *IEEE Transactions on plasma science*, 25(6):1174–1186, 1997. doi:10.1109/27.650894.

[2] P. Picot. *Cahier technique n° 198 La coupure du courant électrique dans le vide*. 2000. URL: http://www.schneider-electric.com.

[3] L. Wang, L. Wang, S. Jia, et al. Experimental study of anode activities in high current vacuum arc subjected to axial magnetic fields under different conditions. *IEEE Transactions on Plasma Science*, 38(7):1682–1691, 2010. doi:10.1109/TPS.2010.2049666.

[4] E. Schade and D. L. Shmelev. Numerical simulation of high-current vacuum arcs with an external axial magnetic field. *IEEE Transactions on Plasma Science*, 31(5):890–901, 2003. doi:10.1109/TPS.2003.818436.

[5] S. Giere, T. Heinz, A. Lawall, et al. Control of diffuse vacuum arc using axial magnetic fields in commercial high voltage switchgear. *Plasma Physics and Technology*, 6(1):19–22, 2019. doi:10.14311/ppt.2019.1.19.

[6] Y. Langlois, P. Chapelle, A. Jardy, and F. Gentils. On the numerical simulation of the diffuse arc in a vacuum interrupter. *Journal of Applied Physics*, 109(11), 2011. doi:10.1063/1.3587180.

[7] B. Tezenas Du Montcel, P. Chapelle, C. Creusot, and A. Jardy. Numerical study of the current constriction in a vacuum arc at large contact gap. *IEEE Transactions on Plasma Science*, 47(5):2765–2774, 2019. Publisher: Institute of Electrical and Electronics Engineers Inc. doi:10.1109/TPS.2019.2909964.

[8] L. Wang, S. Jia, Z. Shi, and M. Rong. Numerical simulation of vacuum arc under different axial magnetic fields. *Journal of Physics D: Applied Physics*, 38(7):1034–1041, 2005. doi:10.1088/0022-3727/38/7/011.

[9] ANSYS. *Ansys Fluent Theory Guide Release 2023 R2*. 2023.

[10] H. Wang, L. Wang, Q. Ma, et al. Experimental investigation of vacuum arc characteristics subject to axial magnetic field contacts with different ratios of diameter to gap distance. *Physics of Plasmas*, 29(11), 2022. Publisher: American Institute of Physics Inc. doi:10.1063/5.0108725.

[11] S. I. Braginskii. *Transport processes in a plasma*. 1965.

[12] J. Kutzner and H. C. Miller. Ion flux from the cathode region of a vacuum arc, 1989, ieee transactions on plasma science. *IEEE Transactions on Plasma Science*, 17(5):688–694, 1989. doi:10.1109/27.41183.

[13] J. Kutzner and H. C. Miller. Integrated ion flux emitted from the cathode spot region of a diffuse vacuum arc. *Journal of Physics D: Applied Physics*, 25(4):686, apr 1992. doi:10.1088/0022-3727/25/4/015.

[14] Y. L. Langlois. *Modélisation de l'arc électrique dans un disjoncteur à vide*. Theses, Institut National Polytechnique de Lorraine, November 2010. URL: https://hal.univ-lorraine.fr/tel-01748841.

[15] C. W. Kimblin. Erosion and ionization in the cathode spot region of vacuum arcs. *J. Appl. Phys*, 44(7):3074–3080, 1973.

[16] J. E. Daalder. Components of cathode erosion in vacuum arcs. *Journal of Physics D: Applied Physics*, 9(16):2379–2395, 1976. doi:10.1088/0022-3727/9/16/009.

[17] C. Simonnet, P. Freton, J.-J. Gonzalez, et al. Influence de la variation de la charge moyenne dans une simulation numérique d'un arc sous vide en présence d'un AMF. *Journal International de Technologie, de l'Innovation, de la Physique, de l'Energie et de l'Environnement*, 9(1), 2025. Number: 1. doi:10.52497/jitipee.v9i1.370.

[18] J. Lowke, J. lPredictions of arc temperature profiles using approximate emission coefficients for radiation losses. *J. Qumt. Spectrosc. Rad. Transfer*, 14:111–122, 1974.

[19] URL: https://hipercone.com/products/kintechdb.

[20] Harvard-smithsonian center for astrophysics, "kurucz atomic and molecular database," cambridge, MA, USA. URL: https://lweb.cfa.harvard.edu/amp/ampdata/kurucz23/sekur.html.

[21] National institute of standards and technology, "atomic spectra database," gaithersburg, MD, USA. URL: https://www.nist.gov/pml/atomic-spectra-database.

[22] M. A. Lieberman and A. J. Lichtenberg. *Principles of Plasma Discharges and Materials Processing*. Wiley, 1 edition, 2005. ISBN 978-0-471-72001-0 978-0-471-72425-4. URL: https://onlinelibrary.wiley.com/doi/book/10.1002/0471724254, doi:10.1002/0471724254.

[23] F. Lago. *Modélisation de l'interaction entre un arc électrique et une surface: application au foudroiement d'un aéronef*. PhD thesis, Toulouse 3, 2004.